Observation of an acoustic non-Hermitian topological Anderson insulator

Zhongming Gu[1,5], He Gao[2,5], Haoran Xue[3⋆], Di Wang[1], Jiamin Guo[1], Zhongqing Su[2], Baile Zhang[3,4⋆] and Jie Zhu[1⋆]

[1]Institute of Acoustics, School of Physics Science and Engineering, Tongji University, Shanghai 200092, China.
[2]Department of Mechanical Engineering, The Hong Kong Polytechnic University, Hung Hom, Kowloon, Hong Kong SAR, China.
[3]Division of Physics and Applied Physics, School of Physical and Mathematical Sciences, Nanyang Technological University, Singapore 637371, Singapore.
[4]Centre for Disruptive Photonic Technologies, Nanyang Technological University, Singapore, 637371, Singapore.
[5]These authors contributed equally: Zhongming Gu, He Gao
⋆e-mail: haoran001@e.ntu.edu.sg; blzhang@ntu.edu.sg; jiezhu@tongji.edu.cn.

The interplay between band topology and disorder can give rise to intriguing phenomena. One paradigmatic example is the topological Anderson insulator, whose nontrivial topology is induced in a trivial system by disorders. In this work, we study the effect of purely non-Hermitian disorders on topological systems using an one-dimensional acoustic lattice with coupled resonators. Particularly, we construct a theorectical framework to describe the non-Hermitian topological Anderson insulator phase solely driven by disordered loss modulation. Then, the complete evolution of non-Hermitian disorder-induced topological phase transitions, from an original trivial phase to a topological Anderson phase, and finally to a trivial Anderson phase, is revealed experimentally through both bulk and edge spectra. Interestingly, the non-Hermitian disorders induced topological modes are also proved to be immune to both the weak Hermitian and non-Hermitian disorders. These results pave the way to the studies on disordered non-Hermitian systems for novel wave manipulation.

topological Anderson insulator, non-Hermitian systems, topological edge states
PACS number(s): 43.20.Fn, 68.35.Rh, 72.15.Rn

1 Introduction

Topological insulators (TIs), exhibiting nontrivial boundary states, are generally immune to weak disorders, while they cannot survive from strong disorders owing to Anderson localization [1]. Surprisingly, it was theoretically discovered that in some cases disorder may also induce, rather than inhibit, topological states [2]. Such disorder-induced topological phases, dubbed topological Anderson insulators (TAIs), have stirred extensive theoretical explorations [2–7] and were experimentally demonstrated in various engineered systems with controlled disorders, including cold atomic wires [8], photonic crystals [9,10], phononic crystals [11,12] and electric circuit [13]. Recently, the concept of TIs was generalized to the open systems described by non-Hermitian Hamiltonians, which possess exotic features without Hermitian counterparts [14], such as non-Hermitian skin effect [15] and modified bulk-boundary correspondence [16, 17]. These intriguing properties of non-Hermitian systems contribute to generating unique topological phenomena that were rarely studied in Hermitian systems. One natural question is how disorder and topology can interact with each other under non-Hermitian settings. Some theoretical explorations reveal the possibilities of realizing non-Hermitian TAIs [18–24]. More recently, it was experimentally demonstrated that a TAI phase can be realized in a non-Hermitian system with Hermitian disorders (i.e., disorders on the Hermitian components of a non-Hermitian Hamiltonian) [25] and in an originally Hermitian system with non-Hermitian disorders (acoustic gain and loss) [26]. But actually, the gain medium is challenging to be obtained, which greatly hinders the practical demonstrations of the non-Hermitian devices.

In this work, we theoretically study a non-Hermitian TAI model in a purely lossy configuration and experimentally realize it in engineered acoustic metamaterial lattices through ingeniously controlling on-site sound dissipations. When suitable non-Hermitian disorder is added to a trivial Hermitian lattice, the system enters a topological phase with the appearance of topological edge states. We also explore the robustness of these topological modes by adding the random Hermitian and non-Hermitian disorders, respectively. These results demonstrate the possibilities to switch the topological phase merely by introducing disordered on-site dissipations, which is easily achieved and can be straightforwardly generalized to various systems in different dimensions. Distinct from the experimental demonstrations of Hermitian TAIs, the strengths of on-site non-Hermiticities can be flexibly tuned with external approaches, without reshaping the lattice structures, which greatly simplify the realizations of TAIs and may push them to practical applications.

2 Theoretical model

We start by considering a one dimensional (1D) Su-Schrieffer-Heeger (SSH) chain [27], as illustrated in Figure 1(a). A finite-sized SSH chain contains N pairs of sites (labeled A and B atoms) with alternating intracell and intercell hopping

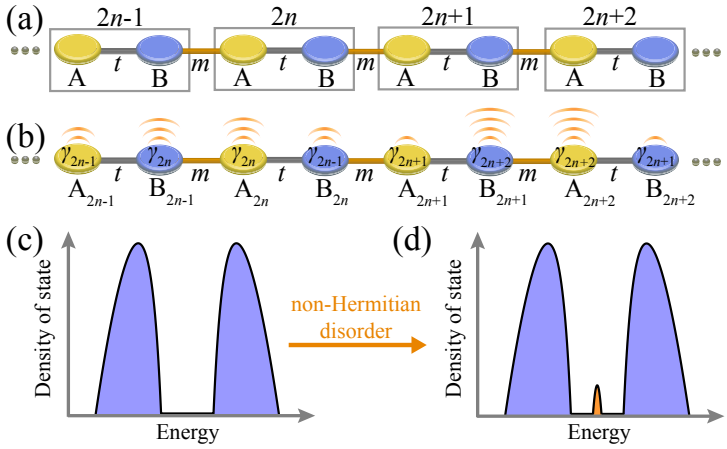

Figure 1 1D SSH chain in periodic Hermitian and disordered non-Hermitian systems. (a) Schematic Hermitian SSH model. Each unit cell has two sites, A and B, with the intracell and intercell coupling amplitudes being t and m, respectively. (b) Schematic SSH model with disordered non-Hermitian staggered potential. The non-Hermitian disorder strengths on sites A_{2n-1} and B_{2n}, B_{2n-1} and A_{2n} are γ_{2n-1}, γ_{2n} $(n = 1, 2, \cdots N/2)$, respectively. (c), (d), Illustrations of the density of state for the finite-sized SSH lattices in (a) and (b), respectively, where $t > m$.

amplitudes (denoted by t and m). When $t > m$, this system is trivial with no states can be found in the gap region, as sketched in Figure 1(c). Such a trivial phase can be turned into a topological one by changing the coupling strength [28] or adding disorders to the couplings [11]. Here, however, we show another approach to drive a topological phase transition, which relies on disorders applied to the on-site dissipations. As presented in Figure 1(c),(d), the non-Hermitian disorders can close the trivial bandgap and opens a topological one with the emergence of in-gap edge states.

The non-Hermitian disorder configuration is shown in Figure 1(b), with the corresponding Hamiltonian reads:

$$\begin{aligned} H = &\sum_{j=1}^{N}(tc^{\dagger}_{B,j}c_{A,j} + \text{H.c.}) + \sum_{j=1}^{N-1}(mc^{\dagger}_{A,j+1}c_{B,j} + \text{H.c.}) \\ &- \sum_{j=1}^{N/2}(i\gamma_{2j-1}(c^{\dagger}_{A,2j-1}c_{A,2j-1} + c^{\dagger}_{B,2j}c_{B,2j}) \\ &+ i\gamma_{2j}(c^{\dagger}_{B,2j-1}c_{B,2j-1} + c^{\dagger}_{A,2j}c_{A,2j})), \end{aligned} \tag{1}$$

where $c^{\dagger}_{A/B,j}$ $(c_{A/B,j})$ is the creation (annihilation) operator on site $(A/B, j)$, γ_{2j-1} (γ_{2j}) is additionally introduced loss to atom A (B) in the $(2j-1)$th unit cell and atom B (A) in the $2j$th unit cell. The non-Hermitian parameter γ_{2j-1} and γ_{2j} $(j = 1 \ldots N/2)$ are uniformly distributed within the interval $[-0.5W, 0]$ and $[-1.3W, -0.8W]$, respectively, with W being the disorder strength. This disordered loss configuration enables the unequally effective reduction of coupling strengths between different sites. Under this disorder configuration, the Hamiltonian has a pseudo-anti-Hermiticity symmetry, which is crucial for defining the topological invariant for this system (see Supporting Information).

3 Quantized topological phase

To clearly show the disordered non-Hermiticity induced topological phase transition, we calculate the bulk polarization for the disordered system. The polarization P_x in real space for 1D system is defined as [24, 29, 30]

$$P_x = \frac{1}{2\pi}\text{Im}\{\log[\det(U_l^{\dagger}\hat{Q}U_r)\sqrt{\det(\hat{Q}^{\dagger})}]\}. \tag{2}$$

where $\hat{Q} = \exp(i2\pi\hat{x}/N)$, $\hat{x}$ is the coordinate operator, and N is the lattice size. U_l and U_r are the occupied and normalized left and right eigenstates (real part of the eigenvalues is less than zero), respectively.

Figure 2(a) shows the calculated phase diagram of a lattice with 200 sites, determined by the non-Hermitian disorder strength W and the intracell coupling t. In all the calculations, the intercell coupling m is fixed to be 1. The intracell coupling $t = 1$ is the critical point between the trivial and topological phase for the clean Hermitian system. When $t < 1$, the system is in topological phase ($P_x = 0.5$) without non-Hermitian disorders. From the phase diagram in Figure 2(a), we observe that P_x is robust to weak and moderate non-Hermitian disorders, possessing a quantized topological phase closely around 0.5. As the disorder strength W is increased to sufficient strong, a relatively rapid drop in P_x can be observed, leading to the system driven to be trivial. Surprisingly, the trivial system ($t \geq 1$) in clean limit can be driven to be topological by increasing the non-Hermitian disorder strength W. Here, the averaged polarization P_x along the white dashed line in Figure 2(a) ($t = 1.25$)

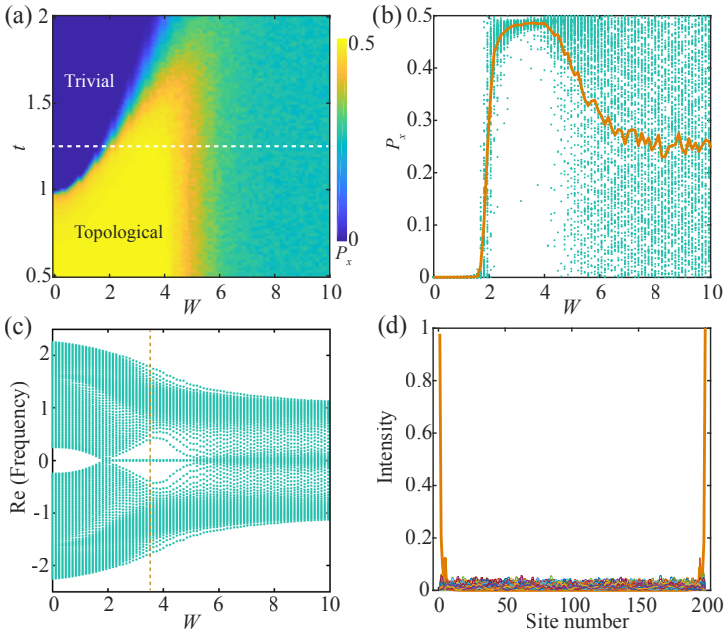

Figure 2 Topological phase transition driven by non-Hermitian disorders. (a) The averaged phase diagram of the model illustrated in Figure 1(b) showing the trivial and topological phases as a function of the intracell coupling amplitude t and non-Hermitian disorder strength W. The intercell coupling amplitude m is fixed to be 1. The polarization P_x is calculated with the lattice size $N = 100$ and averaged over 150 disorder configurations. (b) The numerically calculated polarization P_x versus W along the white dashed line in (a). The cyan dots are the unaveraged data for 150 disorder configurations. The averaged result is denoted by the orange line. (c) The averaged real part of the eigenfrequency as a function of non-Hermitian disorders W. In (b) and (c), the intracell and intercell coupling amplitudes $t = 1.25$ and $m = 1$, indicated by the white dashed line in (a). (d) The averaged intensity profiles for all the eigenstates of the finite-sized lattice with $N = 100$, $t = 1.25$, $m = 1$, and $W = 3.5$ (denoted by the orange dashed line in (c)). All the results are averaged over 150 disorder configurations.

is plotted in Figure 2(b). For weak disorder ($W < 1.8$), the originally trivial system remains to be trivial ($P_x = 0$). With the addition of disorder, P_x sharply rises to approximate 0.5 and maintains around this value for $W < 4.5$. Once the disorder is added to be sufficient strong ($W > 4.5$), the averaged P_x (orange line in Figure 2(b)) rapidly decays to be around 0.25. The cyan dots denote the results for all the 150 samples with strong disorders, which seem to distribute randomly within the range of 0 to 0.5. Such a random distribution of P_x may be attributed to the large number of states near zero energy, making the quantization unavailable [24].

To clearly visualize the topological phase transition, we numerically calculate the eigenspectra as a function of W with $t = 1.25$. As plotted in Figure 2(c), with the increase of the disorder strength, the trivial bandgap gradually narrows and finally closes when W is around 1.8. When W is further increased, a topological bandgap, driven by the moderate non-Hermitian disorders, opens with the appearance of in-gap edge states (see Figure 2(d)). The opened bandgap is gradually enlarged and then narrowed by further adding the disorders. As the non-Hermitian disorders are strengthened to be sufficient strong ($W > 4.5$), the reopened bandgap will vanish, accomplishing with the appearance of a series of modes around zero energy.

4 Experimental implementation

To experimentally implement the non-Hermitian TAI, we fabricated acoustic lattice composed of coupled resonators. Each resonator is a hollow rectangular cavity with dimensions 80 mm × 40 mm × 10 mm. The coupling between adjacent resonators is enabled by a thin channel whose width determines the coupling strength. All the resonators have additional dissipation with disordered strengths, introduced by drilling small holes in the top side of the cavity and inserting sound absorptive materials in the holes (see Figure 3). The loss strength can be flexibly tuned by changing the number and position of the small holes. Here, we design fifteen types of cavities with different losses (from loss level 1 to loss level 15). The spectra for the cavity with all the designed loss are accordingly measured, from which the effective loss factor can be extracted (details see the Supporting Information).

We first fabricate a Hermitian lattice composed of 16 coupled resonators without any disorder. Since the intracell and intercell coupling amplitudes (t, m) of this Hermitian system are designed to be 29.18 Hz and 23.43 Hz, respectively, it is a trivial system without in-gap states, as revealed by the simulated eigenfrequencies in Figure 3(b). We respectively excited and measured the spectrum of each cavity in this lattice, and repeated this process for all the cavities. The measured responses in the edge resonator (the first cavity) and bulk resonator (the ninth cavity) are shown in Figure 3(c). In the edge spectrum (blue line in Figure 3(c)), a gap around 2130 Hz appears, confirming the existence of a trivial bandgap. Similar

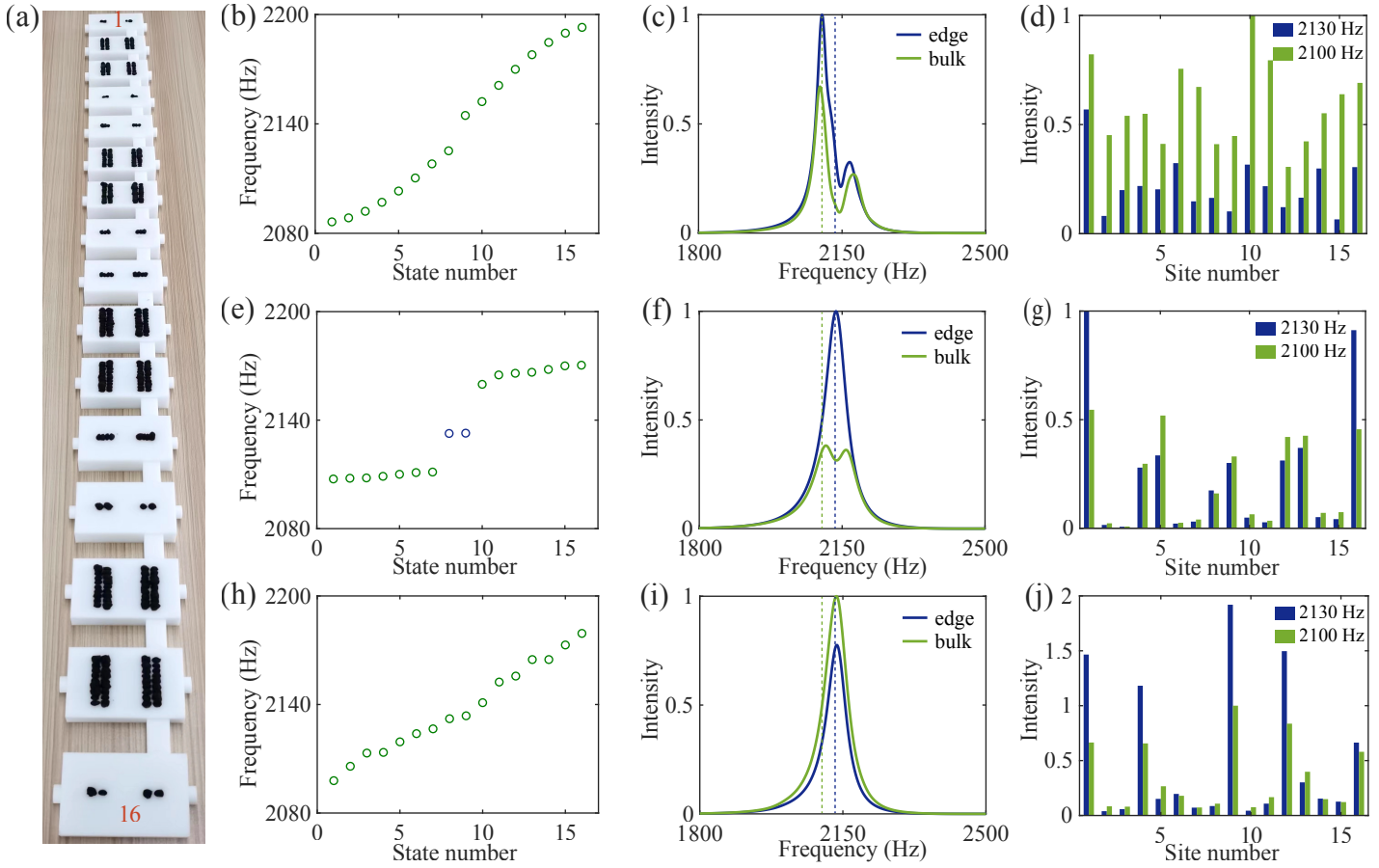

Figure 3 Experimental demonstrations of non-Hermitian TAI. (a), Photo of the experimental sample with moderate non-Hermitian disorder strength. The sample consists of 16 cavities, which are coupled through thin waveguides. The sites with disordered sound dissipations are inserted with different amount of sound absorptive materials. (b), (e) and (h) Simulated eigenfrequency profiles for the lattices without disorder, with moderate disorder and with strong disorder, respectively. (c), (f) and (i) Measured spectra for the lattices without disorder, with moderate disorder and with strong disorder, respectively. The blue line presents the result measured in the first resonator of each sample, while the blue line denotes that in the ninth resonator. (d), (g) and (j) Measured acoustic intensity profiles for the lattices without disorder, with moderate disorder and with strong disorder, respectively. The blue bar and green bar denote the distributions at a frequency being 2130 Hz (indicated by the blue dashed line in (c), (f) and (i)) and 2100 Hz (indicated by the green dashed line in(c), (f) and (i)), respectively.

spectrum is observed in the bulk resonators, as indicated by the green line in Figure 3(c). Furthermore, we measured the acoustic intensity profiles for the whole lattice at the frequency around the dip (2130 Hz) and the left peak (2100 Hz) in the bulk spectrum. We can see that the sound energy is almost uniformly distributed throughout all the sites for these two frequencies, while the intensity for 2100 Hz is higher than that for 2130 Hz (Figure 3(d)). Both the simulation (Figure 3(b)) and experimental measurements (Figure 3(c) and 3(d)) clearly confirm this system to be trivial without the existence of topological edge states.

Now we proceed to explore how to apply the non-Hermitian disorders to the Hermitian lattice for achieving the non-Hermitian TAIs. The expected phase transition process is indicated by the white dashed line in Figure 2(a). We fabricated another two non-Hermitian systems with moderate and strong disorder strengths, respectively. For different non-Hermitian configurations, we can accordingly select the corresponding types of loss from the designed lossy structures. In the two lattices with non-Hermitian disorders, all the cavities are added disordered additional loss, which are implemented with the sound absorptive materials inserting in the small holes. For the lattice with weak non-Hermitian disorder strength, the disorders in the $(4n-3)$th and $4n$th cavities are randomly chosen from loss level 1 to loss level 5, while those for the $(4n-2)$th and $(4n-1)$th $(n=1\ldots4)$ cavities are chosen from loss level 8 to loss level 13. As to the strong non-Hermitian disorder configuration, the disorders in the $(4n-3)$th and $4n$th cavities are randomly chosen from loss level 1 to loss level 7, while those for the $(4n-2)$th and $(4n-1)$th $(n=1\ldots4)$ cavities are chosen from loss level 11 to loss level 15.

The first disordered lattice, as shown in Figure 3(a), has moderate non-Hermitian disorder strength ($W=3.2m$). With this disorder strength, the originally trivial system ($P_x=0$) is driven to be topologically nontrivial ($P_x=0.5$), accompanying with two topological edge states in the bandgap, as depicted in Figure 3(e). Practically, the required loss configurations

are realized by randomly choosing eight types of loss from the designed lossy structures. The spectra in the edge and bulk resonators are measured, respectively, as given in Figure 3(f). We can observe a peak in the edge spectrum (blue line in Figure 3(f)), while there exist two peaks in the bulk spectrum (green line in Figure 3(f)). The gap between the two peaks in bulk spectrum corresponds to the reopened bandgap induced by the disordered non-Hermiticity. The peak with much stronger intensity in the edge spectrum demonstrates the existence of the midgap edge state, around which the intensity profile is denoted by the blue bar in Figure 3(g). At this frequency (2130 Hz), the sound energy is well localized at the two ends of the lattice, very different from the bulk state (2100 Hz), which provides strong evidence for the observation of non-Hermtian TAI. Then, we further increase the non-Hermitian disorder strength W to be around $5m$ (m=23.43 Hz). For this strong non-Hermitian disorder strength, the averaged P_x is around 0.25, and the system is driven to be gapless, as predicted by the numerically calculated eigen spectrum in Figure 3(h). In both the measured edge and bulk spectra (Figure 3(i)), only one peak around 2130 Hz is observed, demonstrating that no bandgap exists in this lattice. We also measured the field distributions in the strong disorder regime, as presented in Figure 3(j). The acoustic intensity at the frequency around the peak of the spectrum (2130 Hz) in Figure 3(i), indicated by the blue bar in Figure 3(j), shows that no apparent energy localization in the boundaries of the lattice can be observed.

5 Robustness of the topological modes

As demonstrated above, the well-tailored non-Hermitian disorder pattern can produce the topological states. For a further step, we will explore whether these disorder induced topological modes can survive under globally random disorders. We first calculated the eigenfrequencies of the non-Hermitian lattice ($W = 3.5$) versus a Hermitian disorder using the according tight-binding model, as presentd in Figure 4(a). The disorder on site i is introduced by changing the real part of the on-site terms as $\mathrm{d}f_i$, uniformly distributed from $-\delta_H$ to δ_H (δ_H is the Hermitian disorder strength). In this case, the frequencies of the edge states remain to be around zero energy for a weak δ_H and then shift towards the bulk bands for large δ_H. In addition, the lattice model is also examined by adding non-Hermitian disorders δ_{NH}, whose eigenfrequency profile is given in Figure 4(b). This disorder is introduced to the on-site term, randomly distributed from $i\delta_{NH}$ to $-i\delta_{NH}$ (δ_{NH} is the non-Hermitian disorder strength). By increasing δ_{NH}, the bandgap gradually narrows, while the zero-energy states remain unchanged before the gap closes. These two cases show that the topological edge states can survive for weak Hermitian and non-Hermitian disorders, demonstrating the robustness of the non-Hermitian TAI.

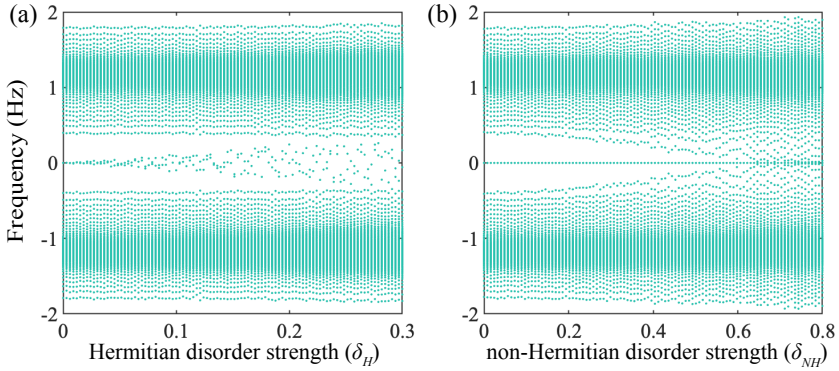

Figure 4 Robustness of the topological edge states. Numerically calculated eigenfrequencies based on the tight-binding model for the non-Hermitian TAI with (a) Hermitian disorder δ_H and (b) non-Hermitian disorder δ_{NH}, respectively.

6 Conclusion

These demonstrated experiments show the exact evolution of a non-Hermitian TAI in acoustic platform simply by using only disspations. Distinct from the Hermitian TAI, non-Hermiticity induced TAI is simply implemented with on-site non-Hermiticity, without changing the dimensions of the site cavities or the coupling waveguides. Specifically, we have presented that an originally trivial system can undergo a phase transition and become topological when the added non-Hermitian disorder is within a moderate region. The induced topological edge states also show the ability of being immune to weak Hermitian and non-Hermitian disorders. When introducing sufficient strong disorders, the system will be driven to be gapless and the non-Hermitian TAI will not hold. The evolution of non-Hermitian TAI phase clearly reveals the complex relationship between disorder, non-Hermiticity and topology, demonstrating the key role of non-Hermitian disorders in exploring topological phases. Since the non-Herimiticity can be flexibly and externally controlled, our experimental demonstrations may facilitate TAI to practical applications. Besides, this scheme can be easily extended to other disordered systems in 1D or higher dimensions, which may boost the experimental realizations of the rich interactions of non-Hermiticity with disorders.

This work was supported by the National Natural Science Foundation of China (Grant No. 92263208), National Key R&D Program of China (Grant Nos. 2022YFA1404400 and 2022YFA1404403) and the Fundamental Research Funds for the Central Universities.

References

1 P. W. Anderson, Absence of diffusion in certain random lattices, Phys. Rev. 109 (5) (1958) 1492.

2 J. Li, R.-L. Chu, J. K. Jain, S.-Q. Shen, Topological anderson insulator, Phys. Rev. Lett. 102 (13) (2009) 136806.

3 C. Groth, M. Wimmer, A. Akhmerov, J. Tworzydło, C. Beenakker, Theory of the topological anderson insulator, Phys. Rev. Lett. 103 (19) (2009) 196805.

4 H. Jiang, L. Wang, Q.-f. Sun, X. Xie, Numerical study of the topological anderson insulator in hgte/cdte quantum wells, Phys. Rev. B 80 (16) (2009) 165316.

5 H.-M. Guo, G. Rosenberg, G. Refael, M. Franz, Topological anderson insulator in three dimensions, Phys. Rev. Lett. 105 (21) (2010) 216601.

6 A. Altland, D. Bagrets, L. Fritz, A. Kamenev, H. Schmiedt, Quantum criticality of quasi-one-dimensional topological anderson insulators, Phys. Rev. Lett. 112 (20) (2014) 206602.

7 P. Titum, N. H. Lindner, M. C. Rechtsman, G. Refael, Disorder-induced floquet topological insulators, Phys. Rev. Lett. 114 (5) (2015) 056801.

8 E. J. Meier, F. A. An, A. Dauphin, M. Maffei, P. Massignan, T. L. Hughes, B. Gadway, Observation of the topological anderson insulator in disordered atomic wires, Science 362 (6417) (2018) 929–933.

9 S. Stützer, Y. Plotnik, Y. Lumer, P. Titum, N. H. Lindner, M. Segev, M. C. Rechtsman, A. Szameit, Photonic topological anderson insulators, Nature 560 (7719) (2018) 461–465.

10 G.-G. Liu, Y. Yang, X. Ren, H. Xue, X. Lin, Y.-H. Hu, H.-x. Sun, B. Peng, P. Zhou, Y. Chong, et al., Topological anderson insulator in disordered photonic crystals, Phys. Rev. Lett. 125 (13) (2020) 133603.

11 F. Zangeneh-Nejad, R. Fleury, Disorder-induced signal filtering with topological metamaterials, Adv. Mater. 32 (28) (2020) 2001034.

12 H. Liu, B. Xie, H. Wang, W. Liu, Z. Li, H. Cheng, J. Tian, Z. Liu, S. Chen, Acoustic topological anderson insulators, arXiv preprint arXiv:2111.06520 (2021).

13 W. Zhang, D. Zou, Q. Pei, W. He, J. Bao, H. Sun, X. Zhang, Experimental observation of higher-order topological anderson insulators, Phys. Rev. Lett. 126 (14) (2021) 146802.

14 V. Martinez Alvarez, J. Barrios Vargas, M. Berdakin, L. Foa Torres, Topological states of non-hermitian systems, Eur. Phys. J. Spec. Top. 227 (12) (2018) 1295–1308.

15 S. Yao, Z. Wang, Edge states and topological invariants of non-hermitian systems, Phys. Rev. Lett. 121 (8) (2018) 086803.

16 T. E. Lee, Anomalous edge state in a non-hermitian lattice, Phys. Rev. Lett. 116 (13) (2016) 133903.

17 F. K. Kunst, E. Edvardsson, J. C. Budich, E. J. Bergholtz, Biorthogonal bulk-boundary correspondence in non-hermitian systems, Phys. Rev. Lett. 121 (2) (2018) 026808.

18 D.-W. Zhang, L.-Z. Tang, L.-J. Lang, H. Yan, S.-L. Zhu, Non-hermitian topological anderson insulators, Sci. China Phys. Mech. 63 (6) (2020) 1–11.

19 X.-W. Luo, C. Zhang, Non-hermitian disorder-induced topological insulators, arXiv preprint arXiv:1912.10652 (2019).

20 H. Wu, J.-H. An, Floquet topological phases of non-hermitian systems, Phys. Rev. B 102 (4) (2020) 041119.

21 H. Liu, Z. Su, Z.-Q. Zhang, H. Jiang, Topological anderson insulator in two-dimensional non-hermitian systems, Chin. Phys. B 29 (5) (2020) 050502.

22 L.-Z. Tang, L.-F. Zhang, G.-Q. Zhang, D.-W. Zhang, Topological anderson insulators in two-dimensional non-hermitian disordered systems, Phys. Rev. A 101 (6) (2020) 063612.

23 R. Wang, K. Zhang, Z. Song, Anderson localization induced by complex potential, J. Phys. Commun. 5 (9) (2021) 095011.

24 H. Liu, J.-K. Zhou, B.-L. Wu, Z.-Q. Zhang, H. Jiang, Real-space topological invariant and higher-order topological anderson insulator in two-dimensional non-hermitian systems, Phys. Rev. B 103 (22) (2021) 224203.

25 Q. Lin, T. Li, L. Xiao, K. Wang, W. Yi, P. Xue, Observation of non-hermitian topological anderson insulator in quantum dynamics, Nat. Commun. 13 (1) (2022) 1–8.

26 Q. Mo, Y. Sun, J. Li, Z. Ruan, Z. Yang, Imaginary-disorder-induced topological phase transitions, Physical Review Applied 18 (6) (2022) 064079.

27 W. Su, J. Schrieffer, A. J. Heeger, Solitons in polyacetylene, Phys. Rev. Lett. 42 (25) (1979) 1698.

28 W. A. Benalcazar, B. A. Bernevig, T. L. Hughes, Electric multipole moments, topological multipole moment pumping, and chiral hinge states in crystalline insulators, Phys. Rev. B 96 (24) (2017) 245115.

29 C.-A. Li, B. Fu, Z.-A. Hu, J. Li, S.-Q. Shen, Topological phase transitions in disordered electric quadrupole insulators, Phys. Rev. Lett. 125 (16) (2020) 166801.

30 W. A. Wheeler, L. K. Wagner, T. L. Hughes, Many-body electric multipole operators in extended systems, Phys. Rev. B 100 (24) (2019) 245135.